INL/JOU-17-43494-Revision-1

Peridynamic Bond-Associated Correspondence Model: Fundamental Aspects and Numerical Behavior

Hailong Chen, Benjamin W Spencer

February 2019

The INL is a U.S. Department of Energy National Laboratory
operated by Battelle Energy Alliance

INL/JOU-17-43494-Revision-1

Peridynamic Bond-Associated Correspondence Model: Fundamental Aspects and Numerical Behavior

Hailong Chen, Benjamin W Spencer

February 2019

Idaho National Laboratory
Idaho Falls, Idaho 83415

http://www.inl.gov

Prepared for the
U.S. Department of Energy
Office of Nuclear Energy, Office of Nuclear Energy
Under DOE Idaho Operations Office
Contract DE-AC07-05ID14517, DE-AC07-05ID14517

Peridynamic Bond-Associated Correspondence Model: Stability and Convergence Properties

Hailong Chen* and Benjamin W. Spencer

Fuels Modeling and Simulation Department, Idaho National Laboratory, Idaho Falls, ID 83402

Final version available as:

H. Chen and B. W. Spencer. Peridynamic bond-associated correspondence model: Stability and convergence properties. *International Journal for Numerical Methods in Engineering*, 117(6):713–727, Feb. 2019. https://doi.org/10.1002/nme.5973

Abstract

The correspondence approach is a powerful technique that permits the usage of standard constitutive models from local theory within a peridynamic formulation. However, the conventional correspondence formulation suffers from material instability, i.e. zero-energy modes, that must be controlled for it to be applied in practice. The recently-introduced correspondence reformulation based on the use of a bond-associated deformation gradient can inherently remove the material instability. In this paper, we show how the bond-associated correspondence model satisfies the requirement for material stability. The convergence behavior is also examined. The accuracy of this approach is further demonstrated by comparing model predictions against local reference solutions and results from the conventional correspondence model with penalty stabilization for both two-dimensional and three-dimensional problems.

* Corresponding author. *Tel.*: +1 208 526 2542.
E-mail address: hailong.chen@inl.gov (H. Chen), benjamin.spencer@inl.gov (B. Spencer).

Keywords: Peridynamics; Correspondence model; Material Instability; Zero-energy modes; Bond-associated deformation gradient

1. Introduction

Among the variety of peridynamic formulations in the literature, the correspondence material model (also known as the non-ordinary state-based model) is especially attractive due to its ability to incorporate any constitutive relationship from local theory [1]. However, the conventional correspondence material model suffers from some practical difficulties, such as non-invertibility [2]. This non-invertibility can be understood as the existence of many possible deformation states within a material point's family that result in the same force state for a bond. As a consequence, there could be many possible deformation states of the entire body under a given loading that satisfy the equilibrium conditions. This has the practical effect of introducing zero-energy modes of deformation to the model that need to be suppressed.

To take advantage of the correspondence model for nonlinear deformation in fracture modeling, there is a strong need for effective zero-energy control schemes. Recently, Chen [3] proposed an alternative correspondence formulation based on the concept of bond-associated deformation gradient. In contrast to the conventional formulation, the deformation gradient and force state are computed specifically associated with each individual bond in the proposed approach. This bond-associated deformation gradient, which is formulated using deformation states within the bond's proximity rather than the whole family, can better capture the deformation of each individual bond, and inherently removes material instability in the conventional correspondence material model.

In this work, the material stability of the bond-associated correspondence formulation is characterized. Numerical examples are employed to demonstrate the accuracy of the bond-

associated correspondence model. The remainder of this paper is organized as follows: Section 2 presents an extensive review of methods available in the literature for zero-energy mode control for the conventional correspondence model. Section 3 provides a review on the bond-associated correspondence formulation proposed by Chen [3]. Stability of the bond-associated formulation is characterized in Section 4. In Section 5, numerical studies including two-dimensional and three-dimensional examples are presented to examine the convergence behavior and accuracy of this approach. The predictions using the bond-associated correspondence formulation are compared with results from the conventional formulation using the penalty force control scheme and finite element reference solutions. Discussions and conclusions are made in Section 6.

2. Survey of stabilization schemes

As previously mentioned, a particularly useful aspect of the peridynamic correspondence model is its capability to adopt any constitutive relationship from local theory. However, the tendency of this model to exhibit oscillation in solutions induced by zero-energy modes has impeded its widespread adoption. Various remedies for zero-energy mode control are available in the literature, and these methods can be categorized into two major groups: fictitious spring-force based methods [4], [5], [6], [7], and stabilized field state based methods [2], [8], [9], [10], [11]. For methods in both groups, a fictitious force state is introduced in the net force state at a material point. With the addition of this fictitious force state $\underline{\mathbf{T}}_{ZEM}$, the net force state at $\mathbf{X}$ has the form

$$\underline{\mathbf{T}}\left[\mathbf{X},t\right]\langle\boldsymbol{\xi}\rangle = \omega\langle\boldsymbol{\xi}\rangle\mathbf{P}\cdot\mathbf{K}^{-1}\cdot\boldsymbol{\xi} + \underline{\mathbf{T}}_{ZEM}\left[\mathbf{X},t\right]\langle\boldsymbol{\xi}\rangle \tag{1}$$

Several alternative techniques for computing this fictitious force state are summarized below:

Method I - *Stretch based linear local bond force* [7]. In this method, background bonds are included to introduce an additional spring-like interaction to the correspondence force state as

$$\underline{\mathbf{T}}_{ZEM}\left[\mathbf{X},t\right]\langle\boldsymbol{\xi}\rangle = C_I \frac{c\left(|\underline{\mathbf{Y}}|-|\boldsymbol{\xi}|\right)}{|\boldsymbol{\xi}|} \tag{2}$$

where C_I is a control parameter having a small value, typically on the order of 0.01, and c is the micromodulus in the bond-based peridynamic model.

Method II - *Average displacement state based linear nonlocal bond force* [6]. A force term based on the average displacement over all the material points in the horizon is added to the correspondence force state as

$$\underline{\mathbf{T}}_{ZEM}\left[\mathbf{X}\right]\langle\boldsymbol{\xi}\rangle = C_{II}\int_{H_{\mathbf{x}}} \omega\langle\boldsymbol{\xi}\rangle\boldsymbol{\eta}\, dV_{\mathbf{x}'} \tag{3}$$

where C_{II} can have the same value as the control parameter in Method I.

Method III - *Corrected deformation based linear nonlocal bond force* [5]. Similar to the technique widely used to suppress the so-called zero-energy hourglass modes of deformation in classical finite element analysis [12], an additional penalty force term is added to the correspondence force state. This penalty force is proportional to the difference between the actual position of a material point in the current (deformed) configuration and the position predicted by the deformation gradient.

$$\underline{\mathbf{T}}_{ZEM}\left[\mathbf{X}\right]\langle\boldsymbol{\xi}\rangle = -C_{III}\left(\frac{18K}{\pi\delta^4}\right)\left(\left(\mathbf{F}-\mathbf{I}\right)\cdot\boldsymbol{\xi}-\boldsymbol{\eta}\right)\frac{\underline{\mathbf{Y}}}{|\underline{\mathbf{Y}}|}\Delta V_{\mathbf{x}'}\Delta V_{\mathbf{x}} \tag{4}$$

where C_{III} is an hourglass force constant, which was set to 0.015 in Ref. [4], and K is the material's bulk modulus.

In the above fictitious spring-like force methods, a common feature is the use of a stabilization control parameter that is dependent on the material constants and needs to be adjusted properly when nonlinear constitutive models are considered. This adjustment process is not straightforward and calibration of this control parameter is potentially time-consuming [6]. More

importantly, these methods do not resolve the fundamental problem in the correspondence formulation that leads to these zero-energy modes.

Method IV - *Stabilized deformation gradient based force state* [9]. A stabilized deformation gradient is constructed from a weighted average of the displacements within a family as

$$\bar{\mathbf{u}}[\mathbf{X}] = \int_{H_{\mathbf{x}}} \omega\langle\boldsymbol{\xi}\rangle \mathbf{u}' dV_{\mathbf{X}'} \tag{5}$$

The stabilized force state is formulated based on the stabilized deformation gradient. According to the authors, this approach suffers from oscillations in strain and stress fields [9].

Method V - *Bond-stretch informed strain tensor based force state* [10]. Bond strain measures are used to construct peridynamic strain measures as

$$\mathbf{E}_m = \int_{H_{\mathbf{x}}} \omega\langle\boldsymbol{\xi}\rangle \varepsilon_m\langle\boldsymbol{\xi}\rangle \mathbf{H} dV_{\mathbf{x}'} \tag{6}$$

where

$$\varepsilon_m = \frac{1}{2m}\left(\left(\frac{\underline{\mathbf{Y}}\cdot\underline{\mathbf{Y}}}{\boldsymbol{\xi}\cdot\boldsymbol{\xi}}\right)^m - 1\right) \tag{7}$$

consists of bond strain measures inspired by the Seth-Hill strain measures, and

$$\mathbf{H} = \frac{5}{2}\frac{\boldsymbol{\xi}\otimes\boldsymbol{\xi}}{\boldsymbol{\xi}\cdot\boldsymbol{\xi}} - \frac{1}{2}\mathbf{I} \tag{8}$$

is a shape state tensor.

It has been shown analytically that the proposed strain measures can be used to avoid unphysical deformation modes, such as subdomain material collapse, in the correspondence material model. However, for practical problems, it is difficult, if not impossible, to formulate work-conjugate stresses from the derived strain measures, and thus the force state between a pair of interacting material points. The authors are not aware of any work reported based on this approach in the literature thus far.

Method VI – *Higher-order deformation gradient based force state* [11]. In this method, special weight functions for different types of neighboring material points are chosen such that the error in the Taylor expansion of the deformation gradient becomes smaller. Numerically, this is equivalent to introducing higher order deformation gradients. However, these specially designed weighting functions are spatial discretization and horizon size specific, i.e., changing the discretization or horizon size requires recalculation of these weighting functions. Moreover, oscillations still exist in the strain and stress fields obtained using this approach [11].

Method VII - *Non-uniform deformation state based force state* [2], [8]. Based on linearized bond-based peridynamic theory and minimum potential energy principle, the force state resulting from the non-uniform part of the deformation state is

$$\underline{\mathbf{T}}_{ZEM}\left[\mathbf{X}\right]\langle\boldsymbol{\xi}\rangle=\frac{1}{2}\omega\langle\boldsymbol{\xi}\rangle\mathbf{C}\langle\boldsymbol{\xi}\rangle\underline{\mathbf{Z}}\langle\boldsymbol{\xi}\rangle-\frac{1}{2}\omega\langle\boldsymbol{\xi}\rangle\left(\int_{H_{\mathbf{X}}}\omega\langle\boldsymbol{\eta}\rangle\mathbf{C}\langle\boldsymbol{\eta}\rangle\underline{\mathbf{Z}}\langle\boldsymbol{\eta}\rangle\otimes\boldsymbol{\eta}dV_{\mathbf{X}'}\right)\cdot\mathbf{K}^{-1}\cdot\boldsymbol{\xi} \tag{9}$$

where the elastic coefficient tensor is

$$\mathbf{C}\langle\boldsymbol{\xi}\rangle=\frac{c\boldsymbol{\xi}\otimes\boldsymbol{\xi}}{\left|\boldsymbol{\xi}\right|^{3}} \tag{10}$$

with c being the micromodulus in bond-based peridynamic model, and non-uniform deformation state

$$\underline{\mathbf{Z}}\langle\boldsymbol{\xi}\rangle=\underline{\mathbf{Y}}\langle\boldsymbol{\xi}\rangle-\mathbf{F}\cdot\underline{\mathbf{X}}\langle\boldsymbol{\xi}\rangle \tag{11}$$

The stabilization scheme proposed by Silling [2] is a special case of Eq. (9) as

$$\underline{\mathbf{T}}_{ZEM}\left[\mathbf{X}\right]\langle\boldsymbol{\xi}\rangle=\beta\langle\boldsymbol{\xi}\rangle\underline{\mathbf{Z}}\langle\boldsymbol{\xi}\rangle-\omega\langle\boldsymbol{\xi}\rangle\left(\int_{H_{\mathbf{X}}}\beta\langle\boldsymbol{\eta}\rangle\underline{\mathbf{Z}}\langle\boldsymbol{\eta}\rangle\otimes\boldsymbol{\eta}dV_{\mathbf{X}'}\right)\cdot\mathbf{K}^{-1}\cdot\boldsymbol{\xi} \tag{12}$$

where $\beta\langle\boldsymbol{\xi}\rangle$ is the prescribed positive-valued weight function, and a possible value is [2]

$$\beta\langle\boldsymbol{\xi}\rangle=\frac{Gc}{\omega_0}\omega\langle\boldsymbol{\xi}\rangle \tag{13}$$

and

$$\omega_0 = \int_{H_{\mathbf{X}}} \omega\langle\boldsymbol{\xi}\rangle dV_{\mathbf{X}'} \tag{14}$$

All of these zero-energy control schemes share the common feature of introduction of an additional force state. None of these schemes inherently address the source of the material instability in the correspondence formulation. Even with these stabilization schemes, the application of the correspondence model is still limited due to issues brought up by the additional force state and regularity requirement on the spatial discretization. There is a strong need for an effective zero-energy mode control scheme that inherently avoids the material instability in the conventional correspondence material model.

3. Bond-associated correspondence formulation

In a departure from the stabilization scheme discussed in Section 2, Chen [3] recently proposed bond-associated deformation gradients to inherently stabilize the conventional correspondence material model without introducing any additional force state. A brief summary of the bond-associated correspondence formulation is given in this section.

3.1. Bond-associated deformation gradient

For a bond $\boldsymbol{\xi}$, there exist an infinite number of mappings that transform the relative position vector state $\underline{\mathbf{X}}\langle\boldsymbol{\xi}\rangle$ in the reference configuration to the relative position vector state $\underline{\mathbf{Y}}\langle\boldsymbol{\xi}\rangle$ in the current configuration. One possible mapping connecting the two states can be written as:

$$\underline{\mathbf{Y}}\langle\boldsymbol{\xi}\rangle = \mathbf{F}_{\boldsymbol{\xi}} \cdot \underline{\mathbf{X}}\langle\boldsymbol{\xi}\rangle \tag{15}$$

where $\mathbf{F}_{\boldsymbol{\xi}}$ is the deformation gradient for bond $\boldsymbol{\xi}$ connecting material point $\mathbf{X}$ and its neighboring material point $\mathbf{X}'$.

It's clear that the deformation gradient $\mathbf{F}_{\xi}$ defined in Eq. (15) can accurately represent the deformation of bond ξ. However, forming this full deformation gradient is problematic because it has more components than there are constraints for a bond. One way to introduce more constraints but not change the solution such that the mapped deformation of bond ξ differs significantly from the actual solution is to include neighboring deformation states. This can be achieved by using an additional local bond-associated horizon $h_{\mathbf{X}'}$ defined at material point $\mathbf{X}'$ as shown in Figure 1. The set of material points within this horizon that are neighbors of material point $\mathbf{X}$ is used to approximate a bond-associated deformation gradient for bond ξ at material point $\mathbf{X}$. The same approach is applied to bond $-\xi$ at material point $\mathbf{X}'$. This approximated bond-associated deformation gradient is more representative of the deformation experienced by each individual bond than the deformation gradient at each material point based on all the deformation states within the horizon as used in the conventional peridynamic correspondence model, since only the deformation states adjacent to this bond are used in the bond-associated deformation gradient approximation.

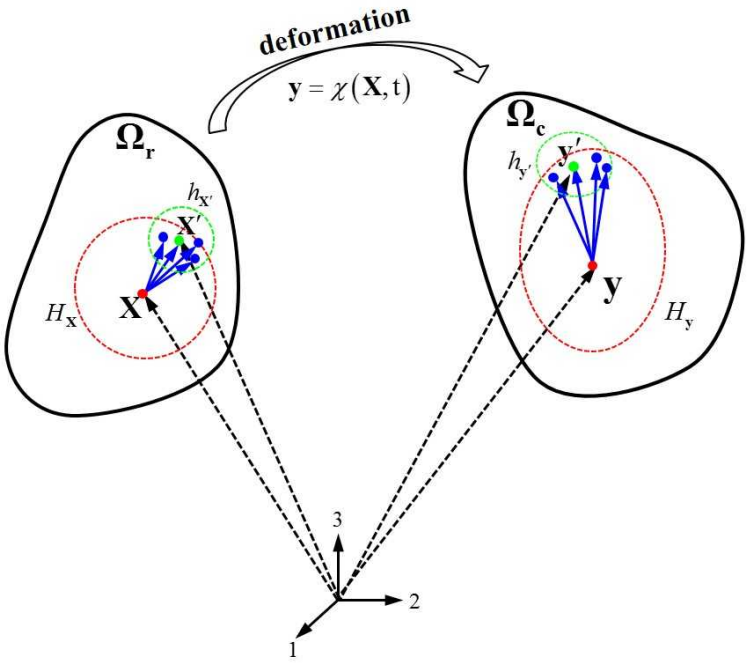

Figure 1. Configuration for bond-associated deformation gradient approximation

Following the same weighted least squares procedure for the material point deformation gradient [3], but using a different integration domain: $H_{\mathbf{X}} \cap h_{\mathbf{X}'}$ rather than $H_{\mathbf{X}}$, the bond-associated deformation gradient for bond $\boldsymbol{\xi}$ at material point $\mathbf{X}$ can be readily obtained as

$$\mathbf{F}^b = \left(\int_{H_{\mathbf{X}} \cap h_{\mathbf{X}'}} \omega\langle\boldsymbol{\xi}\rangle \underline{\mathbf{Y}}\langle\boldsymbol{\xi}\rangle \otimes \underline{\mathbf{X}}\langle\boldsymbol{\xi}\rangle dV_{\mathbf{X}'} \right) \cdot \left(\mathbf{K}^b \right)^{-1} \tag{16}$$

Where $\mathbf{K}^b$ is the bond-associated shape tensor, defined as

$$\mathbf{K}^b = \int_{H_{\mathbf{X}} \cap h_{\mathbf{X}'}} \omega\langle\boldsymbol{\xi}\rangle \underline{\mathbf{X}}\langle\boldsymbol{\xi}\rangle \otimes \underline{\mathbf{X}}\langle\boldsymbol{\xi}\rangle dV_{\mathbf{X}'} \tag{17}$$

It is noteworthy that the derived bond-associated deformation gradient for each individual bond recovers the conventional peridynamic deformation gradient at each material point when the bond-associated horizon size is chosen such that the integration domain is the material point's horizon. In addition, the bond-associated deformation gradient approaches the conventional deformation gradient when the bond approaches an infinitesimal length.

3.2. Bond-associated force state

For the case of the bond-associated deformation gradient, the corresponding force state can be derived following the same procedure outlined in Ref. [1]. At a material point, the bond-associated strain energy density function change $\Delta_{\Delta\underline{\mathbf{Y}}} W^b\left(\underline{\mathbf{Y}}\right)$ due to an increment $\Delta\underline{\mathbf{Y}}$ within its proximity can be determined as

$$\Delta_{\Delta\underline{\mathbf{Y}}} W^b\left(\underline{\mathbf{Y}}\right) = \int_{H_{\mathbf{X}}\cap h_{\mathbf{X}'}} \underline{\mathbf{T}}^b\left(\underline{\mathbf{Y}}\right)\cdot\Delta\underline{\mathbf{Y}}\, dV_{\mathbf{X}'} \tag{18}$$

where $\underline{\mathbf{T}}^b\left(\underline{\mathbf{Y}}\right)$ is the bond-associated force state.

A good approximation of the bond-associated strain energy density from the strain energy density at a material point based on the volume fraction is

$$W^b\left(\underline{\mathbf{Y}}\right) = \frac{\int_{H_{\mathbf{X}}\cap h_{\mathbf{X}'}} 1 dV_{\mathbf{X}'}}{\int_{H_{\mathbf{X}}} 1 dV_{\mathbf{X}'}}\cdot W\left(\underline{\mathbf{Y}}\right) \tag{19}$$

The incremental change in the bond-associated deformation gradient $\Delta_{\Delta\underline{\mathbf{Y}}}\mathbf{F}^b$ is evaluated as

$$\begin{aligned}\Delta_{\Delta\underline{\mathbf{Y}}}\mathbf{F}^b\left(\underline{\mathbf{Y}}\right) &= \mathbf{F}^b\left(\underline{\mathbf{Y}}+\Delta\underline{\mathbf{Y}}\right)-\mathbf{F}^b\left(\underline{\mathbf{Y}}\right)\\ &= \int_{H_{\mathbf{X}}\cap h_{\mathbf{X}'}} \omega\langle\boldsymbol{\xi}\rangle\left(\underline{\mathbf{Y}}+\Delta\underline{\mathbf{Y}}\rightarrow\right)\otimes\underline{\mathbf{X}}\, dV_{\boldsymbol{\xi}}\cdot\left(\mathbf{K}\right)^{-1} - \int_{H_{\mathbf{X}}\cap h_{\mathbf{X}'}} \omega\langle\boldsymbol{\xi}\rangle\,\underline{\mathbf{Y}}\otimes\underline{\mathbf{X}}\, dV_{\boldsymbol{\xi}}\cdot\left(\mathbf{K}^b\right)^{-1}\\ &= \int_{H_{\mathbf{X}}\cap h_{\mathbf{X}'}} \omega\langle\boldsymbol{\xi}\rangle\,\Delta\underline{\mathbf{Y}}\otimes\underline{\mathbf{X}}\, dV_{\boldsymbol{\xi}}\cdot\left(\mathbf{K}^b\right)^{-1}\end{aligned} \tag{20}$$

The bond-associated first Piola-Kirchhoff stress tensor is

$$\mathbf{P}^b \equiv \frac{\partial W^b\left(\underline{\mathbf{Y}}\right)}{\partial\mathbf{F}^b\left(\underline{\mathbf{Y}}\right)} \tag{21}$$

Finally, the bond-associated force state $\underline{\mathbf{T}}^b\left[\mathbf{X},t\right]\langle\boldsymbol{\xi}\rangle$ can be obtained as

$$\underline{\mathbf{T}}^b\left[\mathbf{X},t\right]\langle\boldsymbol{\xi}\rangle = \frac{\int_{H_{\mathbf{X}}\cap h_{\mathbf{X}'}} 1 dV_{\mathbf{X}'}}{\int_{H_{\mathbf{X}}} 1 dV_{\mathbf{X}'}}\omega\langle\boldsymbol{\xi}\rangle\,\mathbf{P}^b\cdot\left(\mathbf{K}^b\right)^{-1}\cdot\underline{\mathbf{X}} \tag{22}$$

The conventional correspondence formulation is exactly recovered when the bond-associated horizon size is chosen such that the integration domain for the bond-associated deformation gradient is the same as the conventional deformation gradient at a material point.

Given Eq. (22), the motion of a material point $\mathbf{X}$ is governed by following equation

$$\rho(\mathbf{X})\ddot{\mathbf{u}}(\mathbf{X},t)=\int_{H_{\mathbf{X}}}\left(\underline{\mathbf{T}}^{b}[\mathbf{X},t]\langle\mathbf{X}'-\mathbf{X}\rangle-\underline{\mathbf{T}}^{b}[\mathbf{X}',t]\langle\mathbf{X}-\mathbf{X}'\rangle\right)dV_{\mathbf{X}'}+\mathbf{b}(\mathbf{X},t),\ \forall(\mathbf{X},t)\in\Omega\times(0,T) \quad (23)$$

where $\rho(\mathbf{X})$ is mass density, $\mathbf{u}(\mathbf{X},t)$ is the displacement vector, and $\mathbf{b}(\mathbf{X},t)$ is external force density vector.

4. Stability of the bond-associated correspondence material model

As was proposed by Silling in Ref. [2], a sufficient stability condition for the conventional peridynamic correspondence material model is

$$d\underline{\mathbf{T}}\Box d\underline{\mathbf{Y}}>0 \text{ for all admissible } d\underline{\mathbf{Y}} \quad (24)$$

Following the same energy minimization presented in Ref. [2], the stability condition for the bond-associated correspondence material model can be expressed as

$$\sum_{b}\left(\frac{\int_{H_{\mathbf{X}}}1dV_{\mathbf{X}'}}{\int_{H_{\mathbf{X}}\cap h_{\mathbf{X}'}}1dV_{\mathbf{X}'}}d\underline{\mathbf{T}}^{b}\Box d\underline{\mathbf{Y}}\right)>0 \text{ for all admissible } d\underline{\mathbf{Y}} \quad (25)$$

In the derivation of the above stability condition for the bond-associated correspondence model, the relationship between bond-associated strain energy density and strain energy density at a material point given by Eq. (19) for is used. At the limit when the bond-associated horizon $h_{\mathbf{X}'}$ is chosen to be large enough such that the bond-associated correspondence formulation recovers the conventional correspondence formulation, i.e. $h_{\mathbf{X}'}=2H_{\mathbf{X}}$ for regular spatial discretization, Eq.(25) becomes Eq.(24).

Each term in the bond-associated formulation in Eq.(25) can be connected to its underlying local material model via the following relationship

$$
\begin{aligned}
&\frac{\int_{H_{\mathbf{X}}} 1 dV_{\mathbf{X}'}}{\int_{H_{\mathbf{X}} \cap h_{\mathbf{X}'}} 1 dV_{\mathbf{X}'}} d\underline{\mathbf{T}}^b \square d\underline{\mathbf{Y}} \\
&= \int_{H_{\mathbf{X}} \cap h_{\mathbf{X}'}} \frac{\int_{H_{\mathbf{X}}} 1 dV_{\mathbf{X}'}}{\int_{H_{\mathbf{X}} \cap h_{\mathbf{X}'}} 1 dV_{\mathbf{X}'}} \left(\frac{\int_{H_{\mathbf{X}} \cap h_{\mathbf{X}'}} 1 dV_{\mathbf{X}'}}{\int_{H_{\mathbf{X}}} 1 dV_{\mathbf{X}'}} \omega \langle \boldsymbol{\xi} \rangle d\mathbf{P}^b \cdot \left(\mathbf{K}^b \right)^{-1} \cdot \underline{\mathbf{X}} \cdot d\underline{\mathbf{Y}} \right) dV_{\boldsymbol{\xi}} \\
&= dP_{ij}^b \int_{H_{\mathbf{X}} \cap h_{\mathbf{X}'}} \left(\omega \langle \boldsymbol{\xi} \rangle dY_i X_p \right) dV_{\boldsymbol{\xi}} \left(K^b \right)_{jp}^{-1} \\
&= dP_{ij}^b dF_{ij}^b = d\mathbf{P}^b \cdot d\mathbf{F}^b
\end{aligned}
\tag{26}
$$

At a material point, based on the definition of the bond-associated deformation gradient and the configuration of bond-associated horizon, it is possible that there exists an incremental deformation state $d\underline{\mathbf{Y}}$ such that $\omega \langle \boldsymbol{\xi} \rangle d\underline{\mathbf{Y}} \langle \boldsymbol{\xi} \rangle = \omega \langle -\boldsymbol{\xi} \rangle d\underline{\mathbf{Y}} \langle -\boldsymbol{\xi} \rangle$, $\forall \boldsymbol{\xi} \in H_{\mathbf{X}} \cap h_{\mathbf{X}'}$, which results in $d\mathbf{F}^b = 0$ for some bond-associated correspondence formulation. However, there will always exist at least one bond-associated correspondence formulation at a material point for which this incremental deformation state $d\underline{\mathbf{Y}}$ results in a nonzero bond-associated deformation gradient, i.e. $d\mathbf{F}^b \neq 0$. Therefore, at each material point, it is guaranteed that Eq.(25) is valid. Thus, the bond-associated peridynamic correspondence material model is stable.

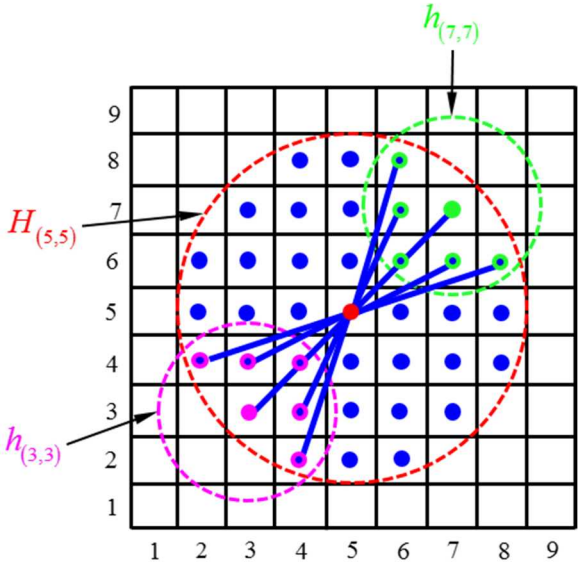

Figure 2. Schematic showing configurations for conventional and bond-associated deformation gradients using regular uniform spatial discretization

To further demonstrate material instability in conventional correspondence model and material stability in bond-associated correspondence model, it is instructive to consider the deformation of a set of points in a horizon shown in Figure 2. Consider a deformation scenario in which an arbitrary displacement $\mathbf{u}'$ is applied to the material point with index (3, 3), and $-\mathbf{u}'$ is applied to the material point with index (7, 7), while fixing all other material points. Under this configuration, the conventional deformation gradient for material point with index (5, 5) can be calculated using Eqs. (16) and (17) but with integration domain $H_{(5,5)}$ as

$$
\begin{aligned}
\mathbf{F}_{(5,5)}\Big|_{\mathbf{u}'_{(3,3)},-\mathbf{u}'_{(7,7)}} &= \left(\sum_{n=1}^{37}\omega\langle\boldsymbol{\xi}_n\rangle\underline{\mathbf{Y}}\langle\boldsymbol{\xi}_n\rangle\otimes\underline{\mathbf{X}}\langle\boldsymbol{\xi}_n\rangle V_n\right)\cdot\mathbf{K}_{(5,5)}^{-1} \\
&= \left(\begin{array}{l}\displaystyle\sum_{n=1}^{37}\omega\langle\boldsymbol{\xi}_n\rangle\underline{\mathbf{X}}\langle\boldsymbol{\xi}_n\rangle\otimes\underline{\mathbf{X}}\langle\boldsymbol{\xi}_n\rangle V_n \\ \underbrace{+\omega\left\langle\boldsymbol{\xi}_{(5,5)\to(3,3)}\right\rangle\mathbf{u}'_{(3,3)}\otimes\underline{\mathbf{X}}\left\langle\boldsymbol{\xi}_{(5,5)\to(3,3)}\right\rangle V_{(3,3)}-\omega\left\langle\boldsymbol{\xi}_{(5,5)\to(7,7)}\right\rangle\mathbf{u}'_{(7,7)}\otimes\underline{\mathbf{X}}\left\langle\boldsymbol{\xi}_{(5,5)\to(7,7)}\right\rangle V_{(7,7)}}_{=\mathbf{0}}\end{array}\right)\cdot\mathbf{K}_{(5,5)}^{-1} \\
&= \left(\sum_{n=1}^{37}\omega\langle\boldsymbol{\xi}_n\rangle\underline{\mathbf{X}}\langle\boldsymbol{\xi}_n\rangle\otimes\underline{\mathbf{X}}\langle\boldsymbol{\xi}_n\rangle V_n\right)\cdot\mathbf{K}_{(5,5)}^{-1} \\
&= \mathbf{1}
\end{aligned}
\tag{27}
$$

Thus, symmetric deformation at symmetric material points with respect to the reference material point in a regular uniform spatial discretization will not result in a change of the deformation gradient in conventional correspondence material model because the effects of the deformation of the two material points are cancelled out. As a result, there is no change in strain energy under this deformation.

However, for the bond-associated formulation under this configuration, all bond-associated deformation gradients for reference material point with index (5, 5) will be non-unity. For example, the bond-associated deformation gradient $\mathbf{F}_{\xi_{(5,5)\to(7,7)}}$ due to the same deformation can be calculated as

$$
\begin{aligned}
\mathbf{F}_{\xi_{(5,5)\to(7,7)}}\Big|_{\mathbf{u}'_{(3,3)},-\mathbf{u}'_{(7,7)}} &= \left(\sum_{m=1}^{np=6} \underline{\mathbf{Y}}\langle\boldsymbol{\xi}_m\rangle \otimes \underline{\mathbf{X}}\langle\boldsymbol{\xi}_m\rangle V_m\right)\cdot\mathbf{K}^{-1}_{\xi_{(5,5)\to(7,7)}} \\
&= \begin{pmatrix} \underline{\mathbf{X}}\langle\boldsymbol{\xi}_{(5,5)\to(7,6)}\rangle \otimes \underline{\mathbf{X}}\langle\boldsymbol{\xi}_{(5,5)\to(7,6)}\rangle V_{(7,6)} + \underline{\mathbf{X}}\langle\boldsymbol{\xi}_{(5,5)\to(6,7)}\rangle \otimes \underline{\mathbf{X}}\langle\boldsymbol{\xi}_{(5,5)\to(6,7)}\rangle V_{(6,7)} \\ + \left(\underline{\mathbf{X}}\langle\boldsymbol{\xi}_{(5,5)\to(7,7)}\rangle - \mathbf{u}'_{(7,7)}\right)\otimes \underline{\mathbf{X}}\langle\boldsymbol{\xi}_{(5,5)\to(7,7)}\rangle V_{(7,7)} \end{pmatrix}\cdot\mathbf{K}^{-1}_{\xi_{(5,5)\to(7,7)}} \\
&= \left(\sum_{m=1}^{np=6} \underline{\mathbf{X}}\langle\boldsymbol{\xi}_m\rangle \otimes \underline{\mathbf{X}}\langle\boldsymbol{\xi}_m\rangle V_m\right)\cdot\mathbf{K}^{-1}_{\xi_{(5,5)\to(7,7)}} - \left(\mathbf{u}'_{(7,7)} \otimes \underline{\mathbf{X}}\langle\boldsymbol{\xi}_{(5,5)\to(7,7)}\rangle V_{(7,7)}\right)\cdot\mathbf{K}^{-1}_{\xi_{(5,5)\to(7,7)}} \\
&= \mathbf{1} - \left(\mathbf{u}'_{(7,7)} \otimes \underline{\mathbf{X}}\langle\boldsymbol{\xi}_{(5,5)\to(7,7)}\rangle V_{(7,7)}\right)\cdot\mathbf{K}^{-1}_{\xi_{(5,5)\to(7,7)}} \\
&\neq \mathbf{1}
\end{aligned}
\tag{28}
$$

The same calculation shown in Eq. (28) can be applied to all other bonds associated with material point with index (5, 5). In the bond-associated formulation, the same deformation that resulted in zero strain energy in the conventional formulation changes the bond-associated deformation gradients, and hence results in a nonzero strain energy.

From the above demonstration, it is clear that this symmetric deformation will have an effect on the bond-associated deformation gradients. Force states resulting from these deformation

gradients will be activated to balance the deformation. Therefore, in contrast to the conventional correspondence model, no zero-energy modes exist in the bond-associated correspondence material model.

The way that the bond-associated deformation gradient formulation removes zero-energy modes in the peridynamic correspondence material model is analogous to the way that full integration stabilizes continuum finite elements, which require stabilization when integrated with a single point rule [12]. This analogy is illustrated for a 4-node quadrilateral finite element in Figure 3. For the case of 1-point integration, a symmetric deformation such as the one applied in Figure 3 does not affect the deformation gradient when evaluated at the center of the finite element, and results in zero change in the strain energy. The root cause for this zero energy behavior under symmetric deformation is essentially the same as that in the conventional peridynamic correspondence material model. When a full integration scheme is used for the finite element, as shown in Figure 3(b), deformation in these symmetric "hourglass" modes will result in a nonzero deformation gradient at all integration points, which effectively eliminates zero-energy modes. Because the bond-associated deformation gradient for the peridynamic correspondence material model is evaluated independently for each bond, it is analogous to using full integration in finite elements. It results in nonzero strain energy under the hourglass deformation modes that cause instabilities in both under-integrated FEM and the conventional peridynamic correspondence model. It should be noted that although a regular discretization is used for both the FEM and peridynamic models in this demonstration, the same principles apply for non-uniform discretizations, where instabilities are observed without stabilization for both methods.

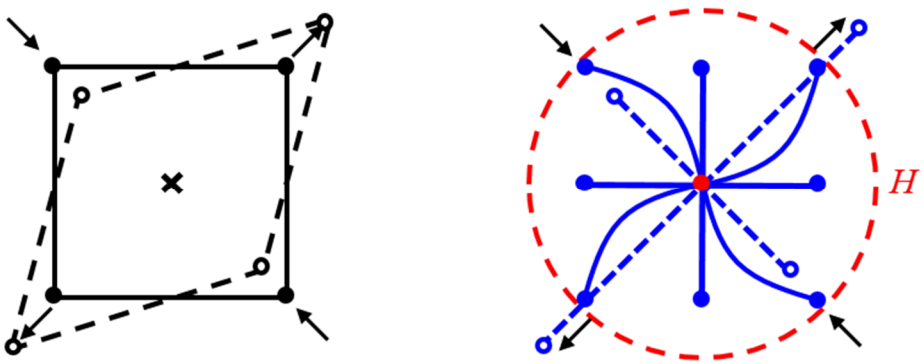

(a). Comparison between 1-point integration in FEM and conventional nodal deformation gradient calculation in the conventional correspondence model under the same symmetric "hourglass" deformation mode. (Both methods have zero strain energy under this mode.)

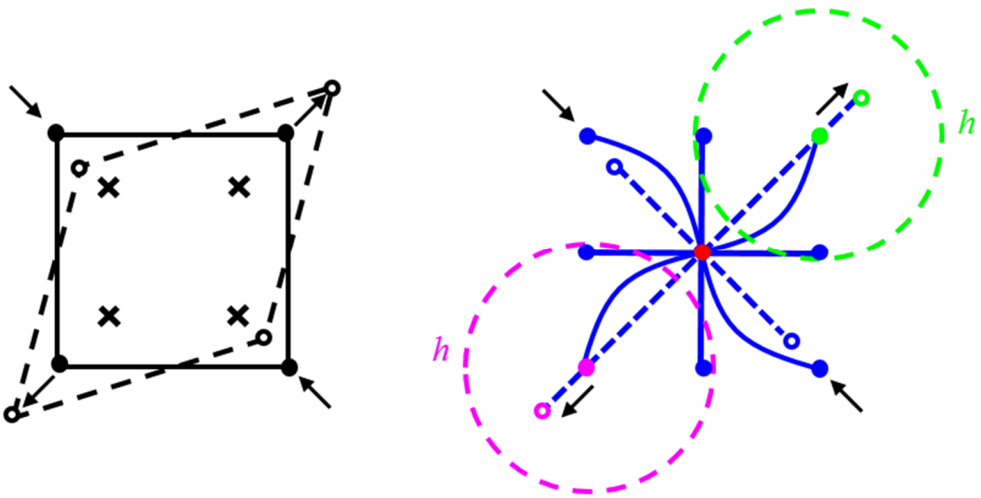

(b). Comparison between 4-point integration in FEM and the bond-associated deformation gradient calculation in peridynamics under the same symmetric "hourglass" deformation mode. (Both methods have nonzero strain energy in this case.)

Figure 3. Illustration of the similarity of the root cause of zero-energy modes in 4-node quadrilateral element in FEM and peridynamic correspondence model using regular spatial discretization (**x**: integration point, —: undeformed shape or bond, ---: deformed shape or bond)

5. Numerical examples

Several examples are studied in this section to further demonstrate the stability and accuracy of the bond-associated correspondence formulation for the simulation of both deformation and fracture. First, a clamped rectangular plate under a point force loading is modeled to demonstrate

the stability and convergence behavior of the bond-associated formulation. Next, detailed comparisons of various deformation measures are made for a three-dimensional rectangular plate with a pre-exiting notch under tensile loading. Finally, the capability of the bond-associated formulation for modeling crack propagation is demonstrated using a two-dimensional rectangular plate with a pre-existing sharp center crack under quasi-static uniaxial tensile loading. For all examples in this section, the same material properties are used: Young's modulus $E = 210$ GPa and Poisson's ratio $v = 0.3$. In all cases, the size of the bond-associated horizon is set to be the same as the size of material point horizon.

Example I: Convergence study using 2D clamped rectangular plate subject to point load

It is well known that peridynamic formulations are non-local and include a length scale determined by the horizon size δ. The peridynamic solution of a problem without spatial singularities approaches the classical local solution as the horizon size δ tends to zero while either keeping the ratio of material point spacing to horizon size m fixed or increasing it at a rate lower than the rate at which δ decreases. On the other hand, for a fixed horizon size δ, as m increases, i.e., the domain discretization is refined, the peridynamic model converges to a nonlocal solution for that horizon size. This non-local solution differs from the classical local solution.

In this example, a clamped rectangular plate subject to a point bending load is utilized to study both the δ-convergence and m-convergence behavior of the bond-associated correspondence formulation. A schematic showing the geometry and loading applied to this plate is shown in Figure 4. Plane strain conditions are assumed in this model. The point force P has a value of 100 kN. The displacement U_y, strain E_{yy} and stress S_{yy} plotted along the neutral axis, denoted as

"axis_1" in Figure 4, are compared for the bond-associated correspondence formulation and a FEM reference solution.

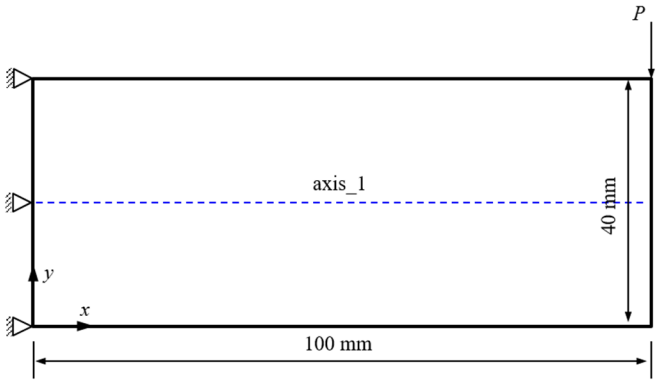

Figure 4. Schematic showing geometry and configuration of a two-dimensional plate

Before investigating convergence characteristics of the peridynamic bond-associated formulation, it is useful to demonstrate the effectiveness of this technique for stabilization on this problem. This problem was run both using a conventional correspondence model without stabilization and the bond-associated correspondence model for comparison. The distributions of displacement U_Y computed using the two approaches are shown in Figure 5. The horizon size is $\delta = 1.5$ mm and $m = 3$. As can be seen, severe oscillations are present in the conventional model prediction, while the bond-associated formulation provides smooth solutions as expected.

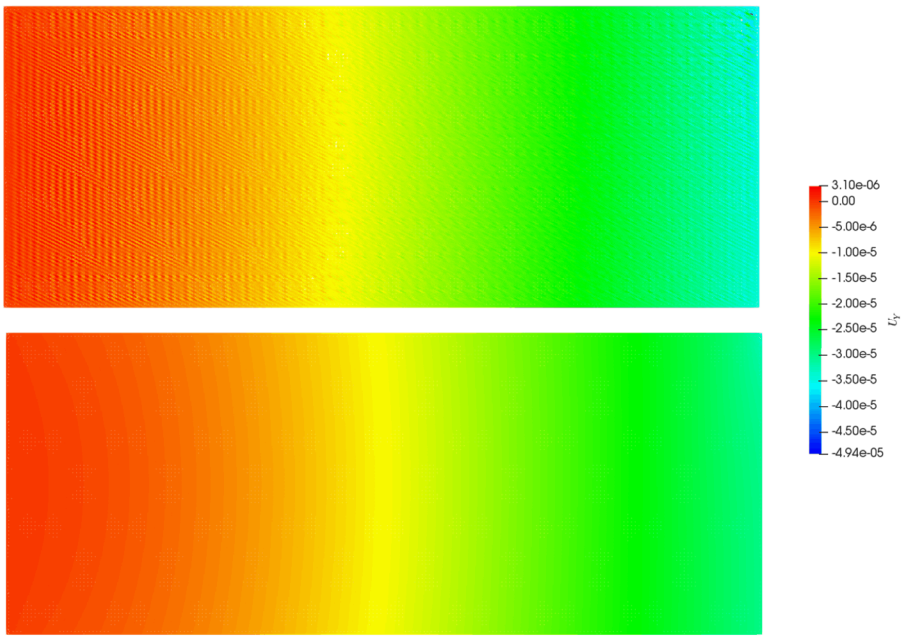

Figure 5. Comparison of displacement distribution prediction between conventional (top) and bond-associated (bottom) correspondence models. (To aid in the comparison of these results, the same color scale is used for both models.)

To study δ-convergence, the value of m is fixed at 3.0. Three values of the horizon size δ are used: 3 mm, 1.5 mm and 0.75 mm. A comparison of selected quantities of interest plotted along the neutral axis for these cases is given in Figure 6. It is evident that as the horizon size δ decreases while keeping the material point spacing factor m fixed, the peridynamic solution converges to the local FEM solution. This is consistent with the convergence behavior of nonlocal peridynamic theory. A horizon size δ = 3.0 mm appears sufficient to accurately capture the deformation of the plate used in this study.

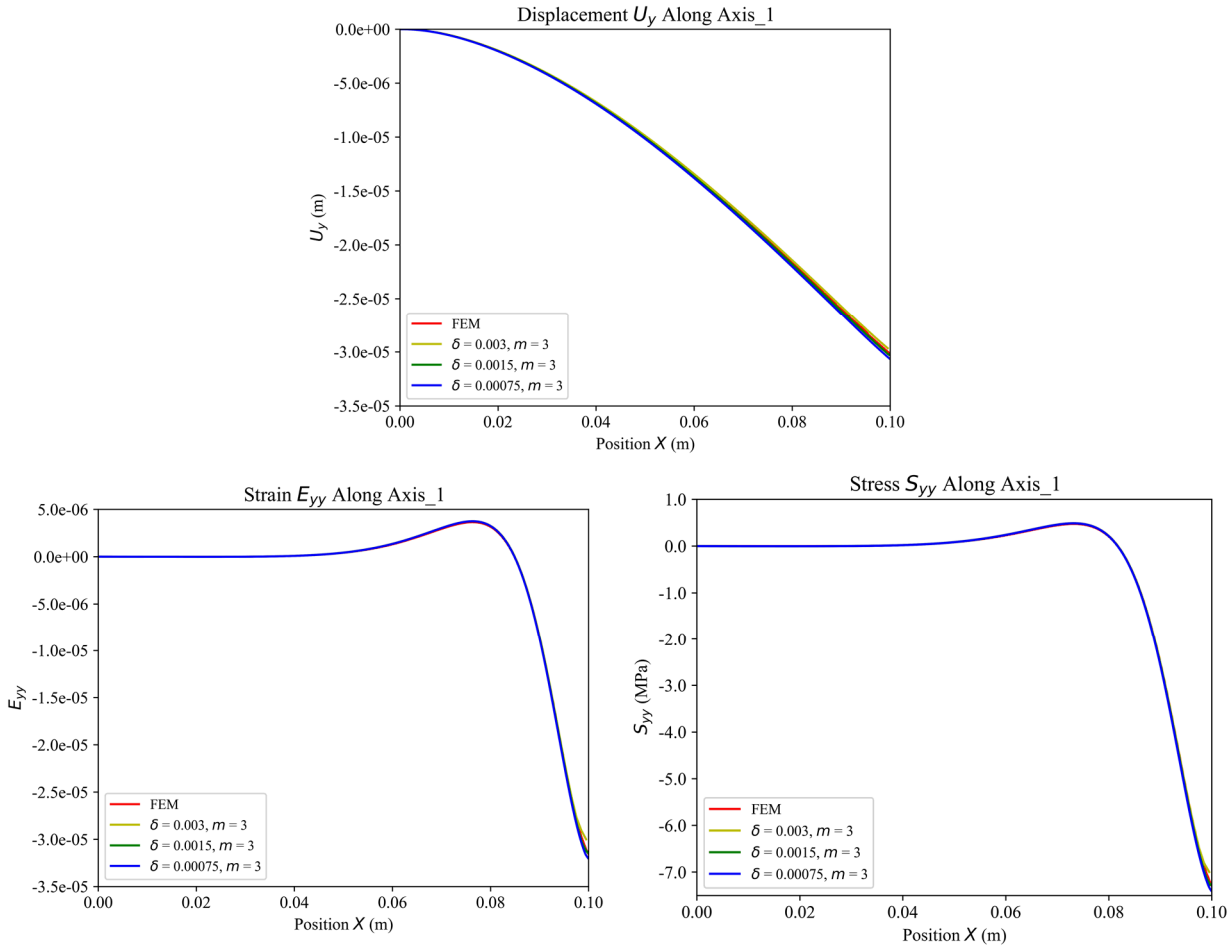

Figure 6. δ-convergence study using two-dimensional plate under point loading

To study m-convergence, the horizon size δ is fixed at 3 mm and m is varied from 3.0 to 5.0. Results for this case are shown in Figure 7, and indicate that the peridynamic solution for $m = 3.0$ best represents the local solution. Increasing m causes the nonlocal peridynamic solutions to begin to differ noticeably from the local solution.

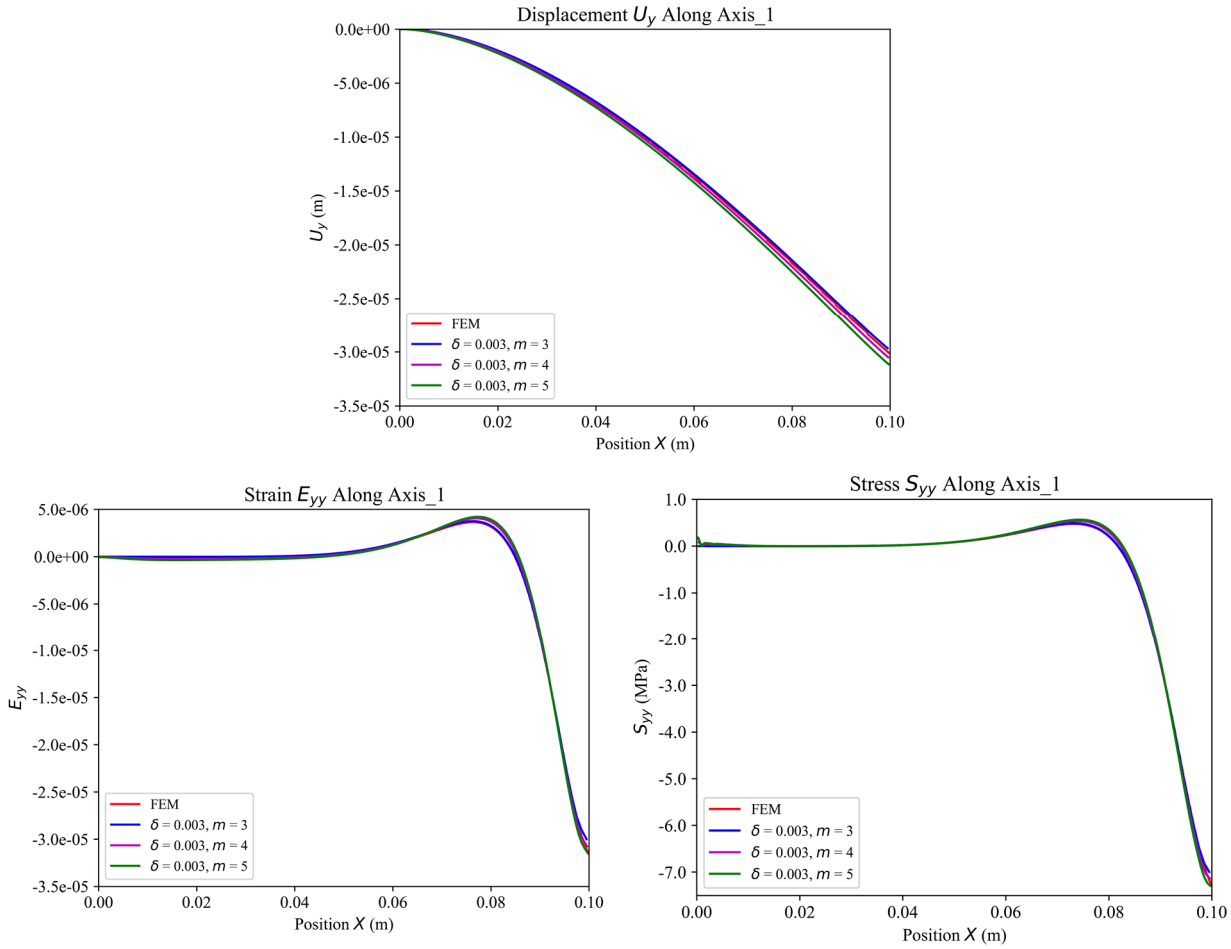

Figure 7. *m*-convergence study using two-dimensional plate under point loading

Example II: Deformation of 3D plate with rectangular notch subject to tension

The next example is designed to further demonstrate the stabilization provided by the bond-associated formulation by comparing it with stabilization method *I* discussed in Section 2 for cases when localized deformation exists. A three-dimensional rectangular plate with a notch in the center is clamped at one end and pulled at the other end with an applied displacement boundary condition. The configuration of the mid-plane of the plate is shown in Figure 8. The out-of-plane thickness of the plate is 10 mm. The applied displacement has a value of 0.4 mm.

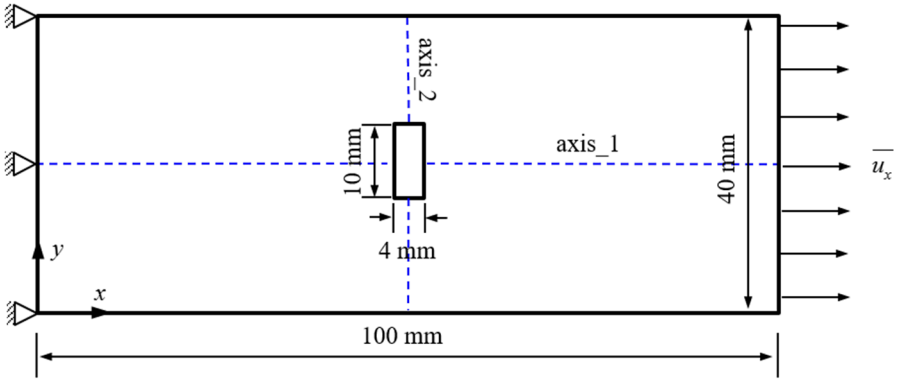

Figure 8. Schematic showing geometry and configuration of the mid-plane of three-dimensional rectangular plate with a center notch

A regular uniform spatial discretization is used with mesh spacing of $\Delta x = 0.5$ mm in all directions, which results in a total of 316,800 material points. Comparisons are made between the conventional correspondence model with stabilization method *I* [7] (denoted as SCI) described in Section 2 and the bond-associated correspondence model (denoted as BAC). Results are also shown for a FEM reference solution.

Comparisons of results plotted along axis_1 and axis_2 on the mid-plane are shown in Figure 9. As can be seen, all of the results from the bond-associated correspondence formulation match quite well with local reference solutions. On the other hand, the SCI formulation shows similar trends but with values that differ significantly from the reference FEM and BAC solutions.

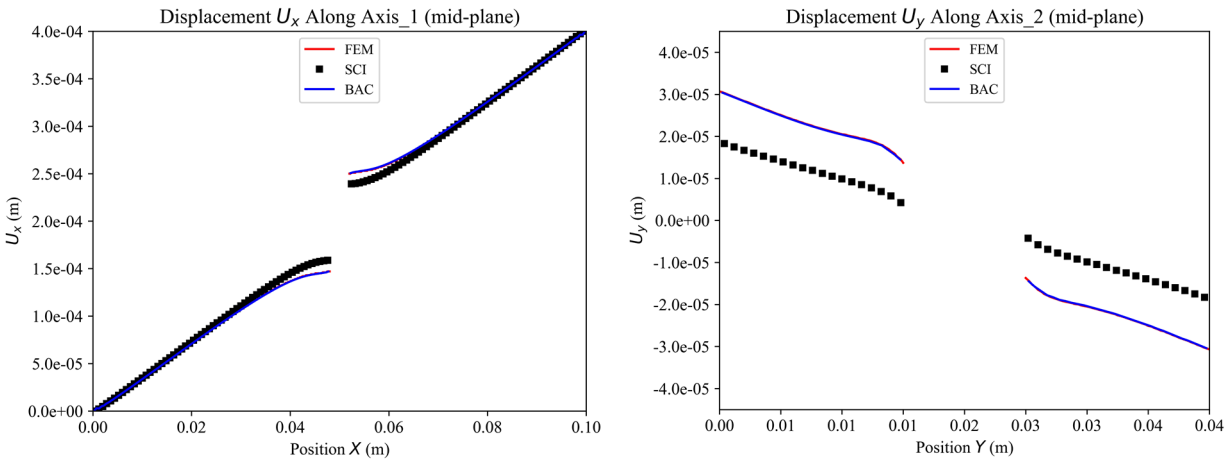

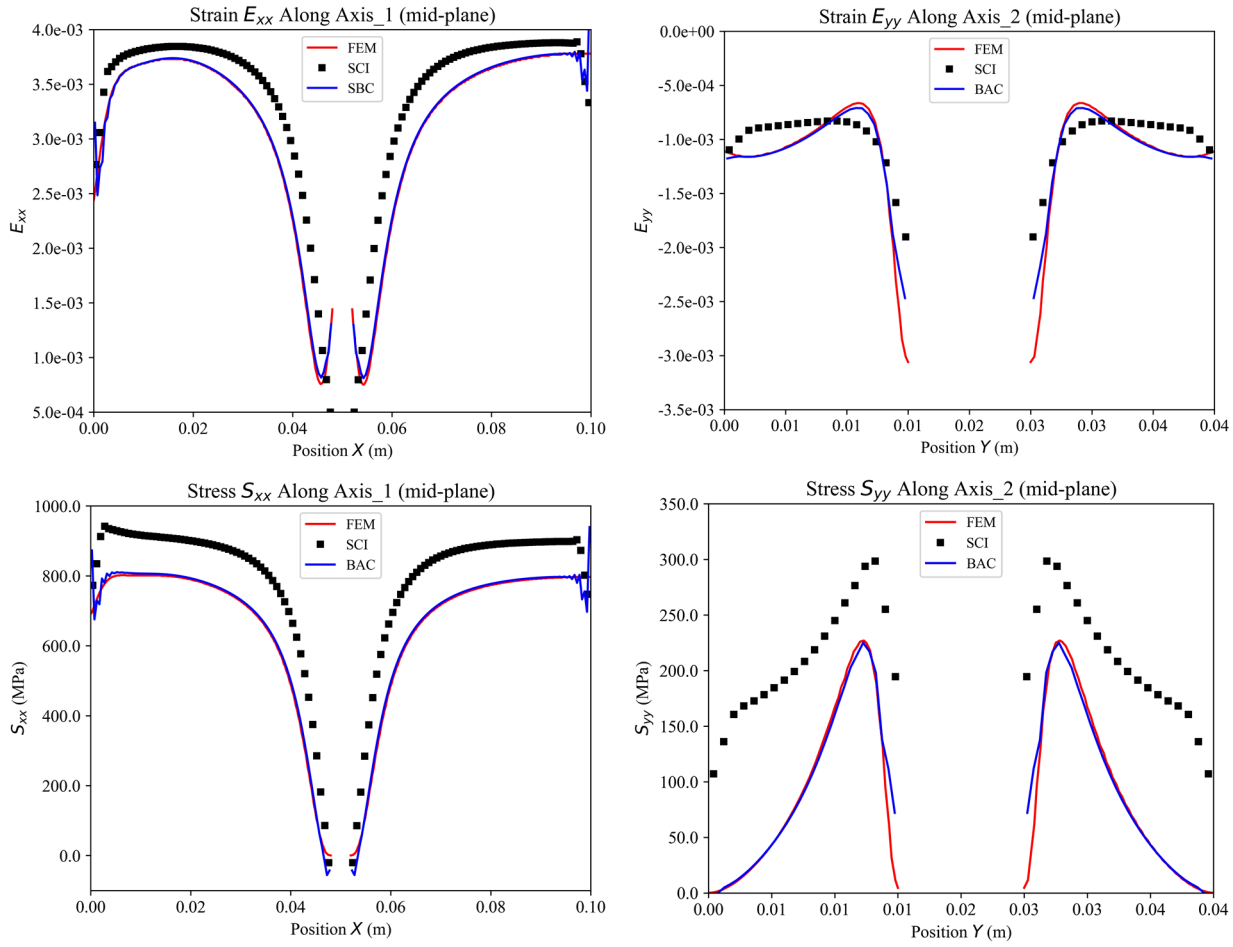

Figure 9. Comparison of quantities of interest for various peridynamic stabilization schemes and FEM reference solution plotted along axis_1 and axis_2 for three-dimensional analysis of center-notched plate

This example demonstrates that the bond-associated correspondence formulation very closely matches a FEM reference solution. It is far more accurate in terms of predicted displacements, strains and stresses for three-dimensional analyses than the other peridynamic stabilization method it was compared against.

Example III: Fracture propagation in 2D plate with pre-existing crack under uniaxial tension

Finally, a two-dimensional fracture example is studied to demonstrate the capability of the bond-associated formulation to model fracture propagation. A rectangular plate shown in Figure 10 with a pre-existing center crack is subjected to uniaxial tension loading. Plane stress conditions

are assumed. A pre-existing sharp crack is represented by removing connecting bonds between material points on each side of the crack surfaces. For simplicity, fracture is assumed to occur when a critical bond stretch criterion is reached, with a critical value of 0.002. This problem was designed to compare to a three-dimensional model in Ref. [2], although a two-dimensional representation is used here.

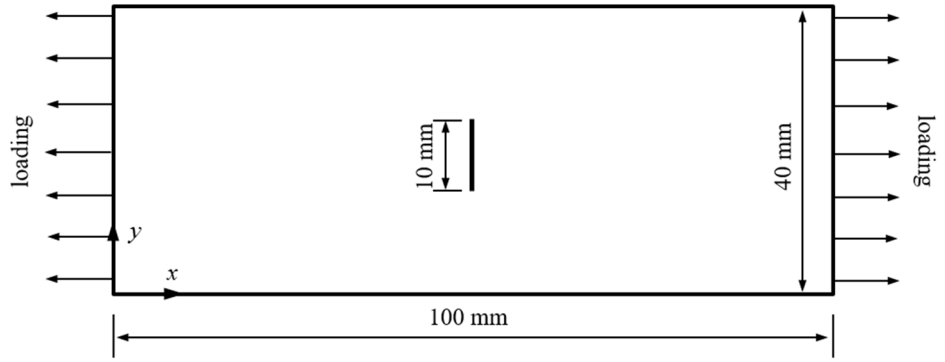

Figure 10. Schematic showing geometry and configuration of a two-dimensional plate

As has been discussed in Ref. [3], the requirement on the minimum number of neighbors should be satisfied to have an invertible, i.e., non-singular, shape tensor and deformation gradient in the bond-associated correspondence model. This also applies to the conventional correspondence model. For deformation analyses without fracture, this requirement can always be met by assigning large horizons, both $H_{\mathbf{x}}$ and $h_{\mathbf{x}'}$, at the beginning of simulation. For fracture modeling, since the horizon sizes should be kept unchanged during the whole simulation, the previously satisfied requirement on the minimum number of neighbors may no longer be satisfied when bond breakage occurs for certain material points. As a result, the shape tensor and deformation gradient may become singular due to this neighbor insufficiency. This scenario is handled in the present work by setting both the shape tensor and bond-associated deformation gradient to the unit tensor when both tensors become singular. With a unit shape tensor and bond-associated deformation gradient, the force state for the corresponding bond becomes zero.

This process essentially treats bonds having a singular bond-associated shape tensor and deformation gradient as being broken in fracture simulations.

It should be noted that since an implicit solution scheme is used throughout this study, the simulation cannot proceed further whenever the Jacobian matrix becomes singular due to the formation of rigid-body modes for material points that are not sufficiently constrained because most of their bonds have failed. This example was run until that occurred, at which time the simulation was terminated.

The damage patterns are shown in Figure 11 at two different simulation time steps to show the paths of crack propagation. As can be seen from Figure 11, the simulated crack paths are qualitatively consistent with expected behavior for Mode-I loading. The finite width of the damage zone is due to the nonlocality of the proposed formulation. This differs from the results shown in Ref. [2], because a control parameter for the localization width was used in that work.

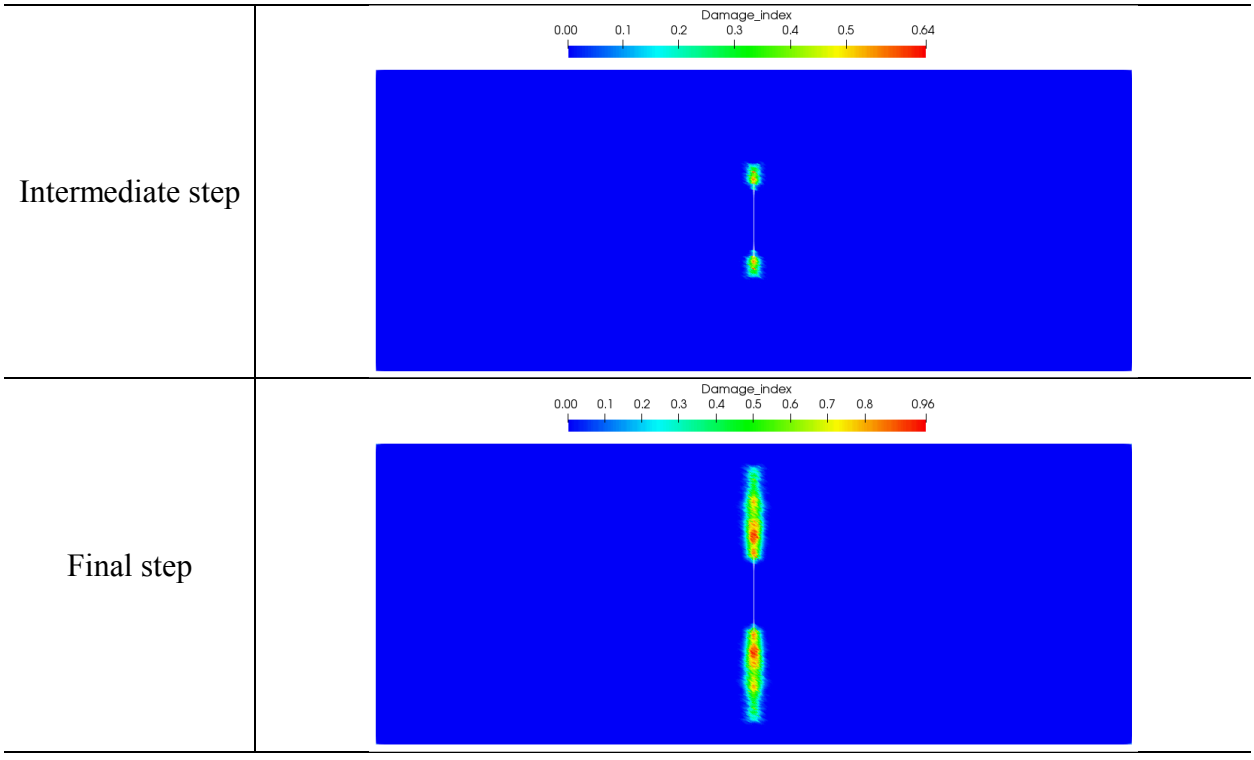

Figure 11. Damage patterns for two-dimensional plate with center crack

5. Discussion and conclusion

A peridynamic bond-associated correspondence formulation can be used to remove material instability, i.e. existence of zero-energy modes, in the conventional correspondence model without the use of external stabilization. A bond-associated deformation gradient is approximated using deformation states within each individual bond's proximity. Material stability of the bond-associated correspondence formulation was analytically characterized. Good convergence behavior of the bond-associated correspondence formulation was demonstrated using a two-dimensional model. Detailed comparisons of several quantities of interest with results from another stabilization method using a three-dimensional plate with a center notch further established the favorable characteristics of the bond-associated correspondence formulation. Finally, the capability of the bond-associated correspondence formulation for fracture propagation was demonstrated using a two-dimensional pre-cracked plate example. For fracture modeling using a simple critical bond stretch criterion in the bond-associated formulation, due to the formulation of the bond-associated deformation gradient and force state, any bond breakage will change the energy at corresponding material points. This is different from the conventional correspondence formulation, in which the usage of critical bond stretch criterion is arguably consistent since certain bond breakage will not change the energy at a material point due to the formulation of deformation gradient at material points, which is similar to the existence of zero-energy modes in conventional correspondence model. The determination of an appropriate critical bond stretch value for the bond-associated correspondence formulation requires additional study.

Acknowledgement

Work supported through the INL Laboratory Directed Research & Development (LDRD) Program under DOE Idaho Operation Office Contract DE-AC07-05ID14517. This manuscript has been authored by Battelle Energy Alliance, LLC under Contract No. DE-AC07-05ID14517 with the U.S. Department of Energy. The United States Government retains and the publisher, by accepting the article for publication, acknowledges that the United States Government retains a nonexclusive, paid-up, irrevocable, world-wide license to publish or reproduce the published form of this manuscript, or allow others to do so, for United States Government purposes.

References

1. Silling, S.A., et al., *Peridynamic States and Constitutive Modeling.* Journal of Elasticity, 2007. **88**(2): p. 151-184.
2. Silling, S.A., *Stability of peridynamic correspondence material models and their particle discretizations.* Computer Methods in Applied Mechanics and Engineering, 2017. **322**: p. 42-57.
3. Chen, H., *Bond-associated deformation gradients for peridynamic correspondence model.* Mechanics Research Communications, 2018. **90**: p. 34-41.
4. Littlewood, D.J., *Simulation of Dynamic Fracture Using Peridynamics, Finite Element Modeling, and Contact.* Proceedings of ASME 2010 International Mechanical Engineering Congress and Exposition, 2010. **9**(44465): p. 209-217.
5. Littlewood, D.J., *A Nonlocal Approach to Modeling Crack Nucleation in AA 7075-T651.* Proceedings of ASME 2011 International Mechanical Engineering Congress and Exposition, 2011. **8**(54945): p. 567-576.
6. Breitenfeld, M.S., et al., *Non-ordinary state-based peridynamic analysis of stationary crack problems.* Computer Methods in Applied Mechanics and Engineering, 2014. **272**: p. 233-250.
7. Bobaru, F., et al., *Handbook of Peridynamic Modeling*. 2016, Boca Raton, FL: CRC Press.
8. Li, P., Z.M. Hao, and W.Q. Zhen, *A stabilized non-ordinary state-based peridynamic model.* Computer Methods in Applied Mechanics and Engineering, 2018. **339**: p. 262-280.
9. Wu, C.T. and B. Ren, *A stabilized non-ordinary state-based peridynamics for the nonlocal ductile material failure analysis in metal machining process.* Computer Methods in Applied Mechanics and Engineering, 2015. **291**: p. 197-215.
10. Tupek, M.R. and R. Radovitzky, *An extended constitutive correspondence formulation of peridynamics based on nonlinear bond-strain measures.* Journal of the Mechanics and Physics of Solids, 2014. **65**: p. 82-92.
11. Yaghoobi, A. and M.G. Chorzepa, *Higher-order approximation to suppress the zero-energy mode in non-ordinary state-based peridynamics.* Computers & Structures, 2017. **188**: p. 63-79.
12. Flanagan, D.P. and T. Belytschko, *A uniform strain hexahedron and quadrilateral with orthogonal hourglass control.* International Journal for Numerical Methods in Engineering, 1981. **17**(5): p. 679-706.